VIV BASED PIEZOELECTRIC ENERGY HARVESTER FOR IOT APPLICATIONS USING HALF CYLINDER

Ahsan Farooq

MUST/FA20-BME-005/AJK

Ali Munir

MUST/FA20-BME-006/AJK

Khawaja Basharat Maqbool

MUST/FA20-BME-016/AJK

Session 2020-2024

Department of Mechanical Engineering

Faculty of Engineering and Technology

Mirpur University of Science and Technology (MUST) Mirpur

AJ&K Pakistan

VIV BASED PIEZOELECTRIC ENERGY HARVESTER FOR IOT APPLICATIONS USING HALF CYLINDER

By

Ahsan Farooq

MUST/FA20-BME-005/AJK

Ali Munir

MUST/FA20-BME-006/AJK

Khawaja Basharat Maqbool

MUST/FA20-BME-016/AJK

A thesis is submitted in partial fulfillment of the requirement for the degree of

BACHELOR OF SCIENCE

In

MECHANICAL ENGINEERING

Session 2020-2024

Department of Mechanical Engineering

Faculty of Engineering and Technology

Mirpur University of Science and Technology (MUST) Mirpur

AJ&K Pakistan

CERTIFICATION

We hereby undertake that this research is an original one and no part of this thesis falls under plagiarism. If found otherwise, at any stage, we will be responsible for the consequences.

Student's Name: **Ahsan Farooq** Signature: _____

Registration No.: **MUST/FA20-BME-005/AJK** Date: 26/08/2024

Student's Name: **Ali Munir** Signature: _____

Registration No.: **MUST/FA20-BME-006/AJK** Date: 26/08/2024

Student's Name: **Khawaja Basharat Maqbool** Signature: _____

Registration No.: **MUST/FA20-BME-016/AJK** Date: 26/08/2024

Certified that the contents and form of thesis entitled **"VIV based piezoelectric energy harvester for IOT Application using half cylinder**" submitted by **"Ahsan Farooq, Ali Munir, Khawaja Basharat Maqbool**" have been found satisfactory for the requirement of the degree.

Supervisor: _____

External Examiner: _____

Date of Viva Voice: 26/08/2024

Chairperson: _____

FYP Coordinator: _____

Dedication

This initiative is dedicated to Allah Almighty, our Creator, a powerful pillar, and a wellspring of wisdom, knowledge, and understanding. Throughout this program, He has been the source of my strength, and I have soared on His wings. Our family is the recipient of our thesis effort as well. We are especially appreciative of our devoted parents, whose words of support and encouragement to persevere never cease to resonate with us. This is also dedicated to my supervisor, who instilled in me the value of perseverance, discipline, and self-focus in order to complete a task.

CONTENTS

LIST OF FIGURES

LIST OF GRAPHS

LIST OF TABLES

Acknowledgement

Praise be to the Lord of all worlds, the Creator of this universe. We are grateful for the strength and passion He has given us to continue our seemingly impossible project. We would like to express our sincere gratitude to **ENGR. DR. M. YAMIN YOUNIS** consultants for the continued support of this project, and his patience, motivation, enthusiasm, and tremendous knowledge. His continuous guidance throughout whole project helped us a lot. He has been an invaluable Bachelor's degree advisor and mentor without which we would not have been able to work effectively on this project.

Secondly, we are grateful to our parents who have been so understanding, caring, and generous with their prayers throughout this very difficult period and of course, all the teachers who have been such a great help and a tremendous source of inspiration.

ABSTRACT

In this work, the performance of a vortex induced vibration energy harvester, coupled with a piezoelectric transducer has been analyzed. Piezoelectric material has been attached with the cantilever beam to harvest energy by freely flapping of cantilever beam in water channel. The materials selected for cantilever beam are silicon steel and stainless steel. Two shapes of bluff bodies, half cylinder without fins and half cylinder with fins, will be used that aided the drag created by the different cut angle and different type of cantilever beam, which creates more heaving of the piezoelectric flag, eventually that leads to more energy harvesting.

Chapter 01

INTRODUCTION

Over past few years energy harvesting has been developed as a sustainable power source technology for wireless sensors and other low level power consuming electronic devices, used in various fields. It eliminates the use of battery packs thus reducing carbon footprints. This technology harvests and converts energy from the environment into usable electrical energy using piezo electric or electromagnetic mechanisms. Energy harvesting systems not only provide sustainable energy but also assist in wireless health monitoring. As research on low-power wireless applications continues to advance, energy harvesting is becoming a major focus of this dissertation.

The energy harvesting through flow structures behind bluff bodies have become significant during past few years in different fields of engineering and in IOT applications. Common shapes of bluff bodies are flat plate, a circle and a square cylinder. These geometries, which are responsible for the turbulent wakes, form composite wake structures behind industrial items like wind turbines, bridges, and cooling towers.

The addition of interactivity of these bodies is the main interest of the studies. The configurations such as tandem and staggered are of great interest to the researchers in this regard. Therefore, the influence of wake relationship in the tandem arrangement of the bluff bodies such as flat plate, round and square is very important. Bluff body can be divided into two main groups. The first group consists of smooth bodies which have no corner cross-section such as elliptical or circle. The second group consists of triangle cross-section, square cross-section and rectilinear cross-section, such as D-shape, which may have a combination of smooth and corner. The shape of the bluff body also plays an important role in the fluid dynamics. Based on the separation points, the two groups above can be separated. The first group of smooth bodies have different separation points. The second group of cornered shapes has fixed separation points. The position of the separation point is very important.The other parameters for flow, e.g., Reynolds number and turbulence intensity. Reynolds number is defined as non-dimensional number which is the

ratio of inertial forces to the viscous forces. Reynolds number is also used to check whether a fluid is laminar or turbulent. It is denoted by Re.

Mathematically,

$$Re = \frac{\rho v d}{\mu} \qquad (1)$$

Where ρ, V, d and μ is density, velocity, diameter and viscosity respectively.

It also takes into account the effects of the specific turbulence model on the measured turbulent wake parameters for a flat plate. Flat plates and cylinders are good examples of bluff bodies that are oriented normal to flow. They have a large area of significant pressure drag and separated flow.

1.1 AIM

To increase the energy harvesting characteristics of piezoelectric material through VIV for IOT application and to study the properties of vibration using different materials.

1.2 OBJECTIVES

- Micro and Nano energy generation using piezoelectric energy Harvesters
- Maximizing the power extracted from a piezo-harvester using Flow Induced Vibration

1.3 METHODOLGY

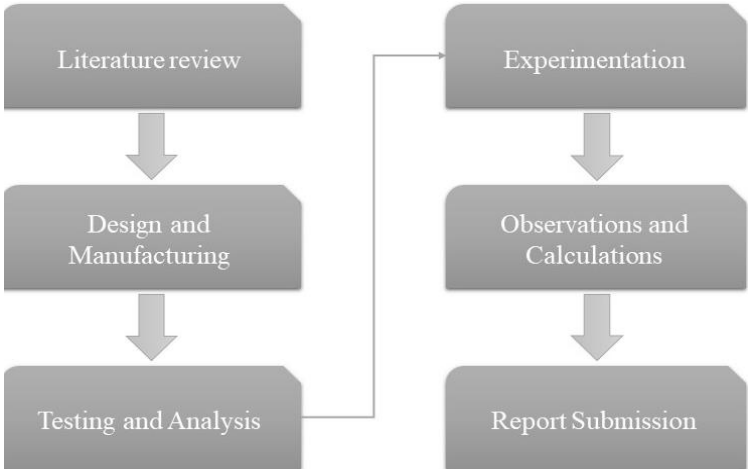

Figure 1.1: Flow chart of methodology of project

1.4 PIEZOELECTRICITY

Piezoelectricity is derived from the Greek word “piezein” translates to “squeeze or press.” Piezoelectricity is the ability of specific materials to produce an electric charge under mechanical stress or pressure and to deform under an electric field. It was first discovered in the late 1800s by French physicist Pierre Curie. The fundamental principle of piezoelectricity is the asymmetric structure of crystal lattices. Natural piezoelectric materials such as quartz and lead zinc zirconate have strong piezoelectric properties, while synthetic piezoelectric materials have more flexibility. The ability to generate mechanical energy and transform it into electrical power is driving innovation and advancing technological capabilities, such as buzzers and actuators, touch sensitive input devices, sensors and energy harvesting.

1.4.1 How Piezoelectricity Works

Piezoelectricity is a phenomenon that occurs when certain materials generate an electric current in response to a mechanical stimulus, such as stress or pressure. This phenomenon is caused by the asymmetric structure of piezoelectric materials. When a material is subjected to mechanical stress, it generates an electric current across the material. Conversely, an electric field on a piezoelectric material causes it to deform or strain because of the rearrangement of charged particles in the piezoelectric lattice. Piezoelectric materials can be either natural (quartz, ceramics, PZT, etc.) or synthetic (polymers, composites, etc.). Piezoelectric materials are used in a variety of applications, from sensors to actuators to transducers to medical imaging devices to energy harvesting systems. The magnitude of the electric charge generated by piezoelectricity depends on the ratio of mechanical stress to electric charge.

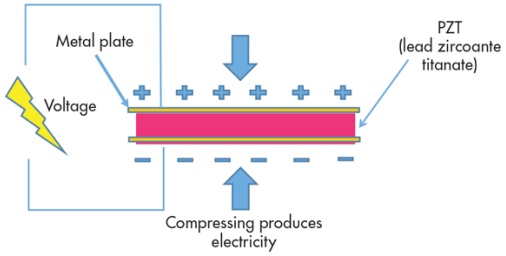

Figure 1.2: Working of piezoelectric material

1.5 AVAILABLE MATERIALS

To improve the oscillations, we have different materials for the cantilever beam as following;

1.5.1 Silicon Steel

Silicon steel, sometimes referred to as electrical steel, transformer steel, is an alloy primarily consisting of iron and silicon, specially designed to have high magnetic permeability (HPM) and low core loss (CRL). This makes it an ideal material for electrical applications, where efficient transfer of energy and low power dissipation are essential. The incorporation of silicon into the steel matrix improves the magnetic properties of silicon steel, which reduces eddy current losses (ECL) and increases electrical resistivity (ESR). As a result, Silicon steel improves the performance and efficiency of electrical equipment, especially in applications with high magnetic flux density (MFD) and frequency.

1.5.2 Stainless steel

Stainless steel resists corrosion, staining and rusting, hence the name “stainless.” It is mainly composed of iron, chrome, nickel, and alloying elements. Its strength and durability make stainless steel a preferred material in many industries. Its resistance to corrosion is due to the presence of a protective layer of chromium oxide on the surface. Its resistance to high temperature, harsh chemicals and physical wear makes it suitable for a wide variety of applications where hygiene, aesthetics and structural integrity are important.

.

Chapter 02

LITERATURE REVIEW

The paper concludes that piezoelectric energy harvesters use the direct piezoelectric effect to generate electrical energy under the influence of mechanical stress. Some of the recent trends and techniques in self-powered devices have been utilizing them. The performance of the piezoelectric energy harvesters depends on numerous factors such as the materials selected, type of configuration, mechanical constraints of materials and structure, and the design of the additional circuitry. A recent trend in piezoelectric energy harvesters has been studied, and the focus of research, techniques used, and their limitations have been tabulated. [1]

The paper concludes that the traditional single-beam wind energy system generates large output power due to vortex shedding, but the harvester remains significant vibration and output for $0 < \theta \leq 22.5$. The proposed bibeam wind EH achieves an omnidirectional wind EH by exhibiting high output energy and a wide range of effectively working speed for all wind directions. The success of the proposed EH is explained by the vibration trajectories of the harvester, which can vibrate in two directions simultaneously. The total displacement responses of the bibeam EH are almost always perpendicular to the approaching wind, leading to considerable cross-wind responses and significant total output power for all wind directions. The performance of the bibeam wind EH and single-beam wind EH has been compared, showing that the proposed bibeam wind EH has overwhelming advantages when the beam is skew to the incoming flow. Both the maximum output power and the range of operating wind speed are maintained at a high level, reinforcing the robustness of the proposed omnidirectional wind EH. [2]

This paper concludes that piezoelectric-energy harvesting has gained popularity in the past two decades, with researchers developing implantable technologies to power portable gadgets and medical equipment. New technologies have enabled the fabrication of highly flexible piezoelectric devices and electronics, leading to the development of biocompatible and long-lasting harvesters. Future work focuses on improving energy-harvesting materials and methods, with circuits needing extra effort to be self-powered. Factors influencing

energy harvester valuation include size, transduction mechanism, and piezoelectric material type. Further research into wind speed and frequency can increase harvester efficiency. Adopters with dual buoys are expected to maximize the performance of piezoelectric generators in wave-energy harvesters using piezoelectric materials. [3]

The paper presents that the response of the energy harvester is quite dependent on the characteristic of the electro-mechanical system and the bluff body cross-section and angle of attack. The load resistance should be tuned to maximize energy production. The rectangular bluff body with b/d = 1.0 at a 0° angle of attack produces the largest vibration amplitude (i.e., largest power output). However, its performances are quite dependent on the angle of attack, resulting in a zero-power output for an angle of attack exceeding 4°. A rectangular bluff body with b/d within 1.62 to 2.5 exhibits a reduced energy production compared with b/d = 1.0 at a 0° angle of attack but better robustness varying the angle of attack. Finally, the trapezium and the angle bluff bodies are not suitable for energy harvesting due to their very high onset velocities within the considered range of angles of attack. [4]

The paper provides a review of energy harvesting techniques from fluid flow using piezoelectric materials. The authors discuss the potential of piezoelectric materials in converting ambient energy into electrical energy, particularly in small electronic devices. The paper also reviews various types of energy harvesting mechanisms based on vibration using piezoelectric materials. The conclusion of the paper is that piezoelectric materials could be used to convert vibration energy into electrical energy in devices that could function in self-powered systems. The paper also highlights the advantages and weaknesses of various types of piezoelectric harvesting devices and materials. [5]

The study found that fluid particles flow reverses in the downstream or wake region due to boundary layer separation and adverse pressure gradient, resulting in eddies. At Re=40, vortex shedding doesn't occur, but at Re=100, flow around a cylinder becomes unstable. The helical system of projecting fins was the most effective device for suppressing vortex induced excitations. The study concluded that helical stacks are the most effective passive vortex control method, reducing vortex shedding frequency dramatically. [6]

The research presents a piezoelectric VIV harvester with a T-shaped design, featuring a fixed bluff splitter body attached to a cantilever PVEH plate. This design increases the aspect ratio for better flow separation and enhances the quality of the generated vortex. Variance in wind speed does not affect the vortex formation length, but it changes the vortex frequency and fluctuating lift force acting on the model. Synchronizing the vortex frequency with the model's natural frequency is crucial for achieving larger vibrational amplitude. The T-shaped VIV energy harvester produces the largest normalized power when the vibrating frequency resonates with the PVEH plate's fundamental natural frequency. Future efforts could focus on lowering the wind speed required to achieve the resonant frequency, improving performance in conventional exhaust air cooling towers. [7]

This study developed a PWEH that integrates VIV and galloping, improving its output performance under fluctuating wind conditions. The design involved a thin-walled bluff body, semicircular wall, and splitter plate. The aspect ratio and non-dimensional afterbody length of the semicircular wall were experimentally investigated. The results showed that the aspect ratio could easily tune flow-induced vibrations. The PWEH experienced VIV, transition from VIV to galloping, and galloping when $2/3 \leq \alpha \leq 4/3$, while only galloping occurred when $3/5 \leq \alpha \leq 2$. Frequency analysis revealed that resonance force and lift instability arose simultaneously, driving the evolutionary process. The non-dimensional afterbody length was crucial for determining galloping behaviors. The proposed wind harvester showed an excellent output power of 30.3 mW at U = 5.0 m/s, sufficient to power small electronics. Future work should focus on visualizing the actual flow field and testing the PWEH's true behavior in natural environments. [8]

This paper presents a high-performance piezoelectric wind energy harvester with Y-shaped attachments (GPEH-Y), which has been verified numerically using the Lattice-Boltzmann CFD method (LBM). The vibrations amplitude of the GPEH-Y increase first and then decrease within a low wind speed range, typical for vortex induced vibrations. For higher wind speeds, the vibrations amplitude continuously increases. The theoretical model of the GPEH-Y is verified through experimental study and theoretical analysis. The study indicates that the Y-shaped attachments on the bluff body can change the aerodynamics characteristic of the PEH. The VIVPEH has a threshold wind speed lower than the GPEH-

Y, and can effectively work in the wind region of 1m/s ⩽U⩽ 1.42 m/s, compared to the GPEH-Y. The GPEH-Y performs better than the GPEH-Square, which was an effective design of galloping energy harvesters. The optimized design and theoretical investigation of the GPEH will be presented in future work. [9]

This paper presents a novel piezoelectric energy harvester, VIVPEH-S, designed to convert vibration mode and enhance energy harvesting efficiency. The system was conceptually designed and experimental prototypes were constructed. The effects of the installation angle of two asymmetrical splitter plates on vibration characteristics and harvesting performance were investigated, and the vortex shedding characteristic and mode conversion mechanism were revealed by CFD simulation. The study found that the installation angles of two asymmetrical splitter plates played a crucial role in improving energy harvesting efficiency. The maximum output voltage of the conventional VIVPEH was limited to 9.93 V at 0.865 m/s to 3.605 m/s. The energy harvesting efficiencies of VIVPEH-S were promoted, and the maximum enhancement ratio of the output power of VIVPEH-S with α =60° and β =90° was up to 471.2% over the conventional VIVPEH. The installation of asymmetrical splitter plates can change the vortex shedding mode, size, and motion state of the vortex. The vortex shedding mode was transformed from the conventional "2S" to "2P" model when α =0° (β =60° and β =120°), and the vortex shedding mode remained as the conventional "2S" model when α =60° and β =90°. [10]

The study examines the performance of a circular cylinder-based wind energy harvester with two small-sized rods of different cross-sectional shapes: a circle, an equilateral triangle, and a square. It found that attaching these rods to the main circular cylinder at θ=45° and 60° sustained power harvesting beyond the critical wind speed, demonstrating superiority over plain circular cylinders and other rod attachment locations. The output voltage for θ=60° was greater than that for θ=45° over the entire working wind speed range. The force measurement results showed that the circular cylinder with triangular rods at θ=60° had the largest transverse force coefficients, confirming the findings in energy harvesting tests. To improve the performance of a circular cylinder-based wind energy harvester, it is recommended to attach two triangular rods parallel to the cylinder axis and symmetrical to the stagnation line, eliminating the upper bound of working wind speed

range in conventional wind energy harvesters. The experimental results provide a basis for developing sustainable, optimized wind-based piezoelectric energy harvesters. Further research is needed to investigate the interaction between vortex-induced vibrations and galloping phenomena using computational fluid dynamics and particle image velocimetry techniques. [11]

This paper presents a cross-coupled dual-beam structure for scavenging wind energy from various incoming directions. Experiments validate the multi-directional capability of the energy harvester. In-depth investigations reveal that different directional wind can cause vortex-induced vibration of different beams. The dominant operation frequencies of the upper and bottom beams differ, with physical explanations provided. The operational wind speed ranges of the two beams are also different, enabling the proposed energy harvester to cover a broader range than traditional wind energy harvesters. The study's underlying mechanisms can inspire other multi-directional designs and provide guidelines for future multi-directional wind energy harvesters. [12]

The study proposes the use of a unimorph piezoelectric cantilever beam for energy harvester applications. The researchers use Euler-Bernoulli beam theory and Hamilton's principle to derive coupled equations of motion and associated boundary conditions under harmonic base excitations. They compute structural natural frequencies and mode shapes accounting for bending-torsion coupling and validate them using FE software Ansys. A reduced-order model of the coupled structural-electrical system is obtained, providing global natural frequencies and mode shapes for the harvester. Closed-form expressions are obtained for displacement, twisting angle, voltage output, and harvested electrical power. A parametric study reveals that the improvement in the harvester's performance increases as the asymmetry increases, with mass distributions increasing harvested power by up to 30%. The study also finds that the lowest two global natural frequencies move closer to each other as the asymmetry increases, suggesting the harvester's ability to harvest power from a broader range of excitation frequencies. [13]

This paper presents a novel piezoelectric energy harvester system for concurrent FIV and VIV, focusing on the coupling effect between FSEH and CBEH. A small wind tunnel was designed and numerous prototypes were manufactured to investigate vibration response

and output characteristics. The study found that longer flexible springs for FSEH reduce the likelihood of FIV, while VIV is easier for CBEH. The vibration response and output performance of various harvesters are mutually enhanced, with enhancing ratios up to 69.6% and 198.3% for FSEH-130-25 and CBEH-130-30, respectively. The output voltage of the harvester increases rapidly, flattens gradually, and decreases with airflow velocity, resulting in a maximum output voltage of 17.94 V for FSEH-140-25 at 13.69 m/s. Field application testing showed a discharging time of 207 s for pedometers. [14]

The paper presents an upright vortex-induced piezoelectric energy harvester (VIPEH) that can convert water energy into electricity. The harvester consists of a PZT cantilever with a cylindrical extension. The energy harvesting ability of the VIPEH is investigated theoretically and experimentally. An Euler-Bernoulli distributed parameter model is established as the available electromechanical model for the energy harvester. The maximum output power of the VIPEH is 84.49 μW with an energy density of 60.35 mW/m2 at a velocity of 0.35 m/s for the configuration I. The energy harvesting ability of the VIPEH increases with reducing the mass M and increasing the diameter D of the cylinder. [15]

EXPERIMENTAL SETUP

3.1 PARTS OF PROJECT

Project consists of following parts:

1) Water Channel
2) Bluff bodies
3) Cantilever beam
    a) Silicon Steel
    b) Stainless Steel

3.1.1 Water Channel

Figure 3.1 illustrates the flow visualization lab of the Department of Mechanical Engineering, School of Mechanical and Manufacturing Engineering (SMME), at the National University of Sciences and Technology (NUST), Islamabad, where experiments are carried out in the High-speed closed-circuit water channel. The behavior of bluff bodies in flow of water is examined by water channel. The water channel has a test section, 2000×400×400 mm (LxWxH). The water tunnel is driven by a centrifugal pump and its RPM is controlled using a variable frequency drive (VFD) motor ranging from 1 to 50 Hz.

Figure 3.1: Water Channel

3.1.2 Bluff bodies

When anything obstructs the flow of a fluid, such air or water, it creates separation and turbulence in its wake. This phenomenon is known in fluid dynamics as a bluff body. When forced to fluid motion, bluff bodies' unique structure produces substantial resistance, in contrast to streamlined bodies, which are meant to reduce drag and promote smooth flow. Bumpy geometric forms such as cubes, spheres, and cylinders are examples of bluff bodies. The shape of a bluff body is such that it creates a high-pressure region in front of it and a low-pressure region behind it.

Here we used two types of bluff bodies i.e. semi-circular cylinder without fins and semi-circular cylinder with fins. The height of the semi-circular cylinder without fins is 3D i.e. 75mm and external diameter of this bluff body is 25mm.When using semi-circular cylinder with fins, the dimension of fins is 0.062D. The height and external diameter of this bluff body is 75mm and 25mm respectively.

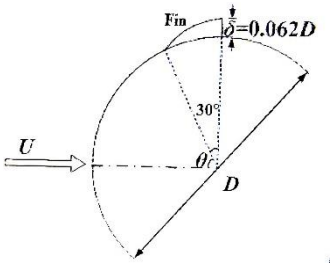

Figure 3.2: Dimensions of fin

The isometric views of both bluff bodies are shown below:

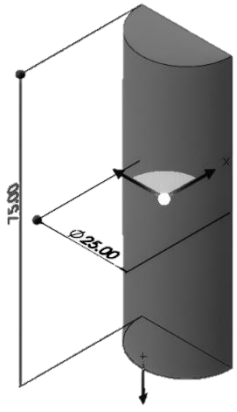

Figure 3.4: Semi-circular cylinder without fins

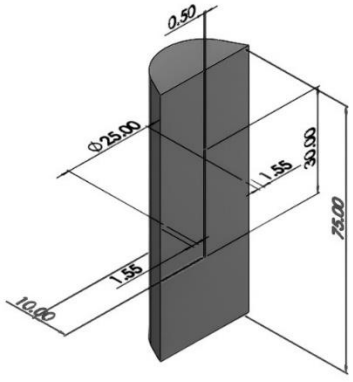

Figure 3.3: Semi-circular cylinder with fins

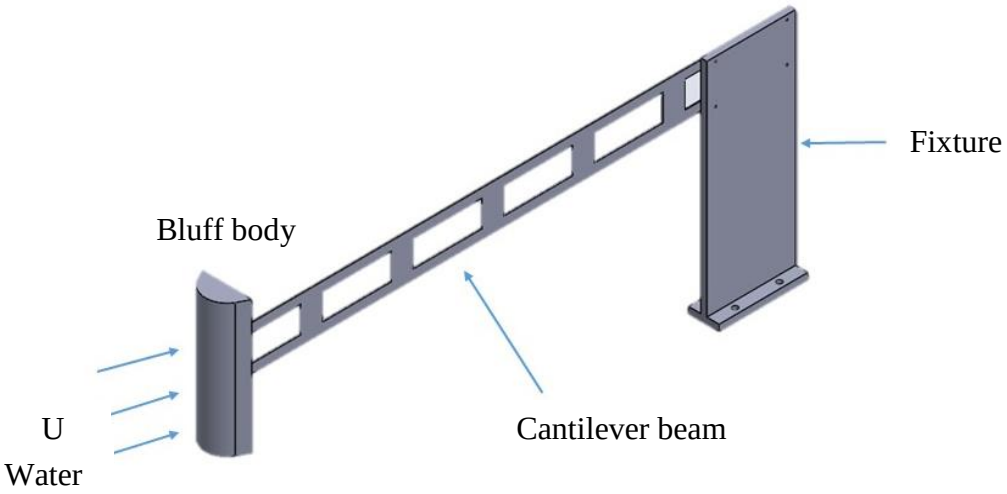

Figure 3.5: 3D schematic of cantilever beam and bluff body with fixture

3.1.3 Cantilever beam

A cantilever beam is a type of structural member that may be fastened at one end and moved freely at the other to create an overhanging shape. The capacity to tolerate loads applied perpendicular to the longitudinal axis and bending moments is a characteristic of cantilever beams. In our work, a bluff body is inserted at the end of this cantilever beam. We use two types of cantilever beams i.e. stainless steel and silicon steel.

a) Stainless steel

Iron, chromium, nickel, and molybdenum are the elements that make up stainless steel, an alloy that resists corrosion. Because of its resistance to corrosion, rust, and stains, it is frequently employed in many different industries. Stainless steel is adaptable for a wide range of applications since it is available in different grades and finishes.

b) Silicon steel

Silicon steel is a specific alloy composed of silicon and iron, also referred to as electrical steel or transformer steel. It's perfect for electrical applications because to its minimal core loss and strong magnetic permeability. Electric motors, generators, transformers, and other electromagnetic equipment frequently employ it.

Table 3.1: Comparison of properties of two cantilever beams

Properties	**Unit**	**Stainless steel**	**Silicon steel**
Length	mm	334.39	334.39
Width	mm	25	25
Thickness	mm	0.5	0.3
Volume	mm^3	4180	2508
Mass	g	31.65	19.14
Density	g/mm^3	0.00757	0.00763

3.2 MASS BALANCING OF CANTILEVER BEAMS

In order to study the vibration properties of different materials, we have balanced the mass of above two cantilever beams by cutting rectangular holes from the one beam of larger mass i.e. stainless steel. We have reduced the mass of stainless steel from 31.65 g to 19.14 g by cutting three rectangular holes. Two rectangular holes have same length and width of 40mm and 12.4mm respectively. One rectangular hole has length and width of 35mm and 12.4mm respectively. This enables to balance mass of both cantilever beams. As a result we will study the behavior of two different cantilever beams having same weight. Mass balancing allows for a fair evaluation of the performance and responsiveness of various beam configurations by ensuring that they are subjected to equal loading circumstances.

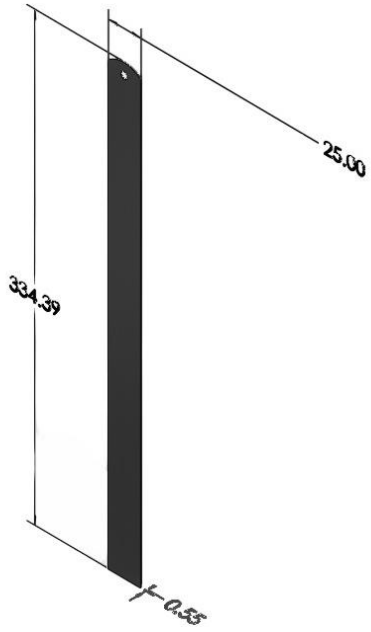

Figure 3.6: Stainless steel before cutting holes

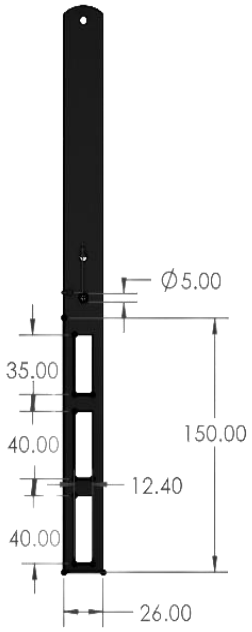

Figure 3.7: Stainless steel after cutting holes

3.3 TESTING

After completing design and manufacturing, we have done testing of our work in water channel at different frequencies of pump. We tested two cantilever beams using two different bluff bodies. One cantilever beam is made up of stainless steel having rectangular holes for length of 150mm and other is made up of silicon steel having length of 150mm. The rectangular holes are covered with thin plastic sheet so that vortices act on equal surface area. Bluff bodies used for testing are already explained above i.e. semi-circular cylinder without fins and semi-circular cylinder with fins. The pump frequencies used for testing are 16Hz, 22Hz, 28Hz, 34Hz and 40Hz. The pump frequency is changed from 16Hz to 40Hz to check which cantilever beam will give maximum flapping. As a result, the cantilever beam having maximum flapping will produce maximum electric current via electric eels for IOT applications.

For each frequency of pump, the video was recorded with high-speed camera (Sony RX100 IV, mounted beneath the test section) for 2 minutes. The cantilever beam of stainless steel

with bluff body semi-circular cylinder without fins was placed inside the water channel where it was fixed on the fixture. It was tested for above mentioned frequencies of pump for 2 minutes each. After 5 cases, the bluff body was replaced with semi-circular cylinder with fins while retaining the same cantilever beam. It was then tested for 5 frequencies of pump. The next step was to replace the stainless steel cantilever beam with silicon steel cantilever beam and to test it for two different bluff bodies in a similar manner as stainless steel. Each case was tested for 2 minutes and video was recorded for each case.

The video recorded for each case is post processed with MATLAB. Frequency and amplitude codes are run in this software to get the required graphs of amplitude and frequency. This post processing gives us frequency and amplitude graphs for flapping of each cantilever beam under different conditions. Comprehending the amplitude and frequency response is essential for optimizing energy production in energy harvesting, which transform vibration into electrical energy. Energy efficiency can be raised by designing the system to function close to a resonant frequency.

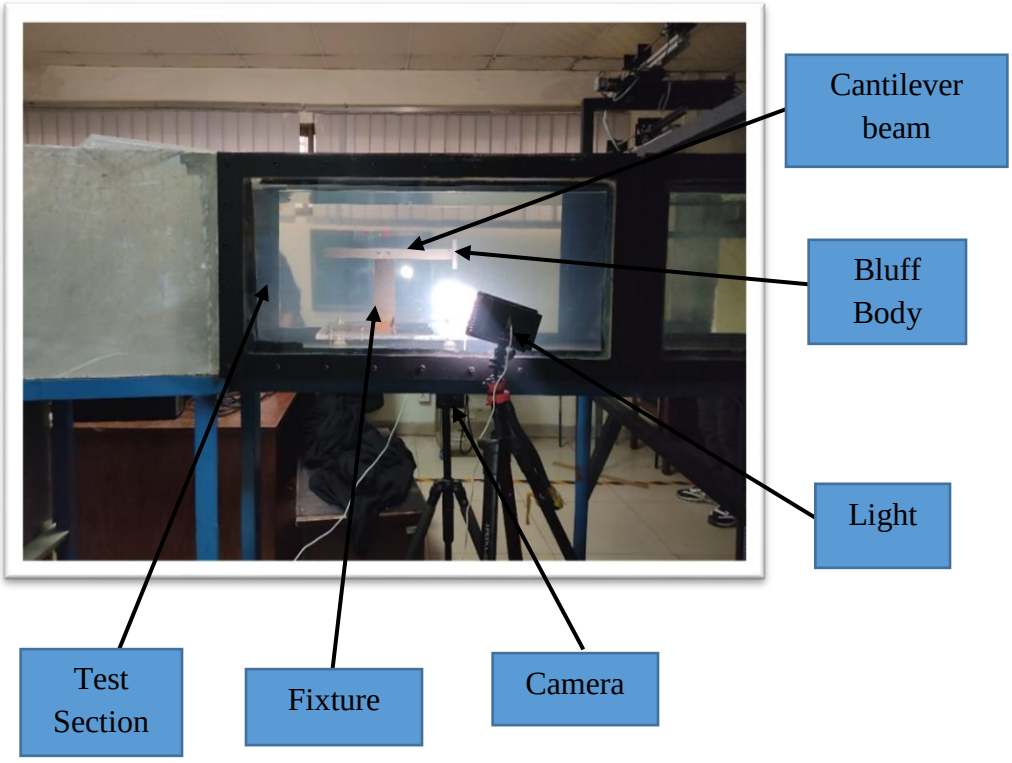

Figure 3.8: Apparatus during testing

3.3.1 Variable Frequency Drive (VFD)

The motor that propels the water flow is controlled by the Variable Frequency Drive (VFD) depicted in the figure 3.9. The VFD is a motor control device that regulates the speed of the motor, allowing for precise control of water velocity within a tunnel. This helps optimize the conditions under which cantilever beams flap, as the efficiency of energy harvesting depends on the frequency and amplitude of the beam's motion, which are directly influenced by flow speed. The VFD's ability to fine-tune water velocity allows researchers to explore different flow regimes and their impact on the cantilever beam's energy harvesting performance.

Figure 3.9: Variable Frequency Drive

3.3.2 Centrifugal Pump

With a 10 horsepower centrifugal pump, the system can flow at a maximum rate of 0.5 meters per second. The voltage regulator was used to determine the minimum water velocity in this low speed water tunnel, which was determined to be 0.15 m/sec. The pump

can achieve a maximum water velocity of 0.55 m/sec in the test section. It reduces flow turbulence. In order to control the flow rate, different ideas on adjusting the input voltage using a VFD controller were looked at. At the moment, a ball valve and a variable speed AC controller are utilized.

Figure 3.10: Centrifugal Pump

3.3.2 Honey Comb Structure

A honeycomb essentially reduces the turbulence caused by the movement of the water. With the exception of accounting for both the frictional resistance and the inertial effect of the fluid mass inside the cell, the first analysis is similar to the classical one for screens. It also makes the assumption that the cell flow has fully developed to the point where transverse fluctuations are completely eliminated. The second analysis includes the turbulence produced in the cell flow if the cell flow is turbulent as well as the turbulence due to wake breaking up behind each cell. The honeycomb construction is made of waterproof aluminum, which guarantees that its use is preserved. The structure of the honeycomb is stabilized and maintains its shape. 1850 x 152.4 x 500 mm are its measurements (L x W x H).

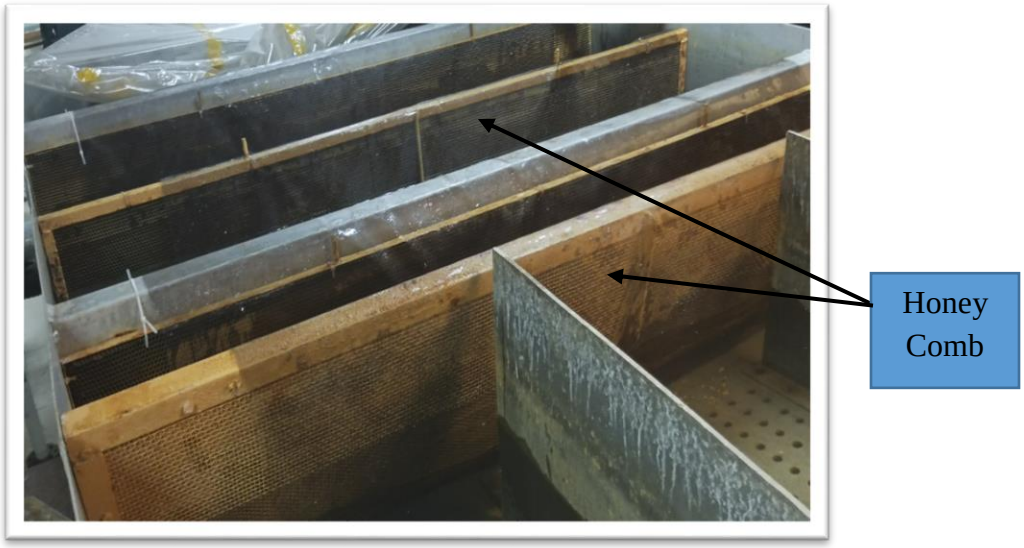

Figure 3.11: Honey Comb Structure

3.4 POST PROCESSING

The post processing of videos is completed in MATLAB software. This software gives the graphs of amplitudes and frequencies when run with relative codes. This process gives values of peak frequency and amplitude for each flapping cantilever beam. This allows us to analyze the best cantilever beam having maximum flapping for generation of electric current for IOT applications.

3.4.1 Codes used in MATLAB to determine frequency and amplitude

Code 1

```
clc;

clear;
close all;


% Batch Processing
video_files = {'11.MP4'};


% Process each video file
```

```
for vid = 1:length(video_files)
    disp('Working on video');
    vidObj = VideoReader(video_files{vid});

    % Read the first frame and crop it
    I = readFrame(vidObj);
    [J, rect] = imcrop(I);     % J is image and rect is
coordinates

    % Initialize variables
    tip_pos = zeros(1, 2);
    cuurentframe = 1;

    % Initialize `ss` to the size of the cropped image
    ss = zeros(size(J));

    vidObj.CurrentTime = 0.0;

    while hasFrame(vidObj)
        F = readFrame(vidObj);
        fprintf('Current    Processing    Frame:\t    %d\n',
cuurentframe);

        % Convert from RGB to Grayscale
        U = rgb2gray(F);

        % Crop frames to desired workspace
        Q = imcrop(U, rect);
```

```
        % Convert cropped image to binary
        W = Q > 180; % Use threshold to create binary image

        % Ensure `ss` has the same size as `W`
        if cuurentframe == 1
            ss = zeros(size(W)); % Initialize `ss` only once
        end

        % Update `ss` with the binary image
        ss = ss | W; % Use logical OR to accumulate the
flapping envelope

        % Extract and process region properties
        regionstats = regionprops(W, 'all');
        if ~isempty(regionstats)
            [~, largestidx] = max([regionstats.Area]); % Find
index of largest region
            h = regionstats(largestidx).Extrema;          %
Coordinates of extreme axis
            pcoor = (h(3,:) + h(4,:)) .* 0.5;             %
Average coordinates
            tip_pos(cuurentframe,:) = pcoor;
        end

        cuurentframe = cuurentframe + 1;
    end

    disp('Done');
```

```
    % Save the results
    xlswrite(strcat(video_files{vid}, '.xlsx'), tip_pos);
    imwrite(double(ss), strcat(video_files{vid}, '.jpg'));
end

% Display the final result
S = double(ss); % Use `ss` directly for the final image
imshow(S);

% Analysis of extrema (example usage)
if ~isempty(h)
    [temp, originalpos] = sort(h(:,1), 'descend');
    max_num = input('Ist ? max. values to read: ');
    n = temp(1:max_num); % Top max values
    p = originalpos(1:max_num); % Indices in original array
    val = h(p,2);

    fprintf('Top values in first column:\n');
    disp(n);
    fprintf('Corresponding values in second column:\n');
    disp(val);
end
% Example loop (just to show loop usage)
for aa = [1, 2, 3]
    disp(aa);
end
```

Code 2

```
%% filtering matlab

clc

clear all

[v] = xlsread('11.MP4.xlsx', 'sheet1','D1:D6200');

dt= xlsread('11.MP4.xlsx', 'sheet1','C1:C6200');

figure(1)

plot(dt,v)

title ('')

xlabel('Time Step')

ylabel('Amplitude')


%% reading of excel file for specified column/values of peak
and lower position of flapping

 data = [v];

%A = [ 65 66 67 68 69 70];

%chr = mat2str ([data]);

A = data'

a = max(A);

b = min(A);

c = [a,b];


xlswrite('Delta-Y.xlsx',c);


%% plot magnitude spectrum of a signal

clc

X_mags=abs(fft(v))

figure(2)
```

```
plot(X_mags)
xlabel('DFT Bins')
ylabel('Magnitude')
%% filter
%plot the first half of normalized frequency
%num_bins = length(X_mags);
num_bins = length(X_mags);
figure(3)
plot ([0:1/(num_bins/2 -1):1] , X_mags(1:num_bins/2))
xlabel('Normalizedd frequency ')  %(\pi rads/sample)
ylabel('E')
%% reading of excel file for specified column/values of
voltages
 data = X_mags;
%A = [ 65 66 67 68 69 70];
%chr = mat2str ([data]);
B = data'
C =(B(1,5:end))
d = max(C);
e = min(C);
f = [d,e];


xlswrite('Energy Spectra.xlsx',f);



%%
[b_cheby,a_cheby] = cheby1(9, 0.9, 0.02, 'low');
H_cheby = freqz(b_cheby, a_cheby);
```

```
%plot filter
norm_freq_axis = [0:1/(512 -1):1];
figure(4)
plot(norm_freq_axis, abs(H_cheby),'r')
legend('Chebyshev')
xlabel('Normalised Frequency');
ylabel('Magnitude')
```

RESULTS AND DISCUSSIONS

After post processing of each case we have obtained different results of frequencies and amplitudes for each cantilever beam for varying pump frequency from 16Hz to 40Hz. Peak value of frequency for both cantilever beams with both bluff bodies is determined from 16Hz to 40Hz. Comparisons of bluff bodies mounted to silicon and steel substrates with and without fins are part of the investigation. These findings shed light on how the substrate material and fins affect the flow properties and oscillation behavior in many fluid dynamic circumstances.

4.1 EFFECT OF VARYING PUMP FREQUENCY ON SUBSTRATE'S PEAK FREQUENCY

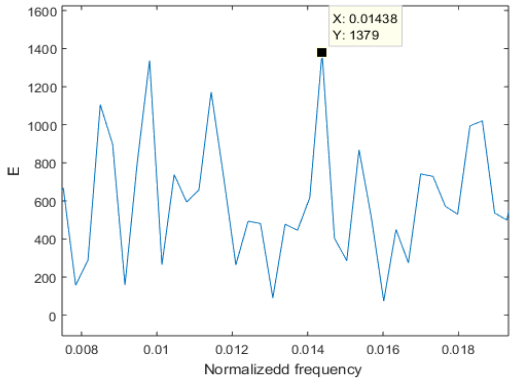

Graph 4.1: Silicon Steel Half Cylinder with Fins at 16Hz

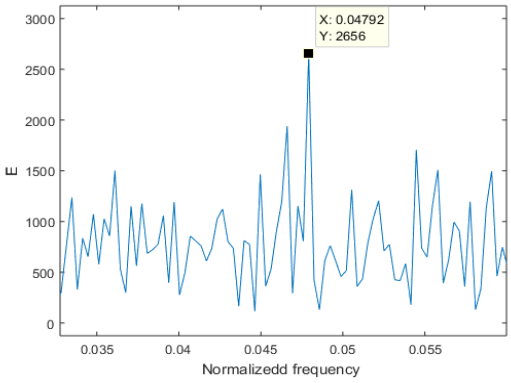

Graph 4.2: Silicon Steel Half Cylinder with Fins at 22Hz

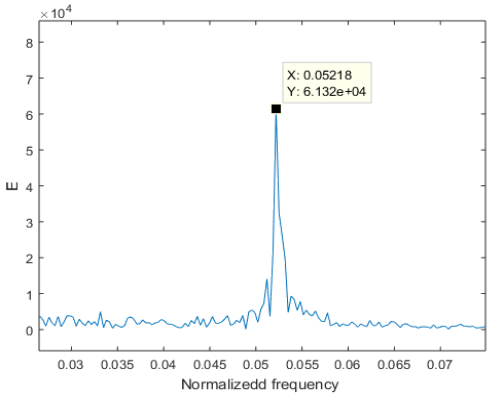

Graph 4.3: Silicon Steel Half Cylinder with Fins at 28Hz

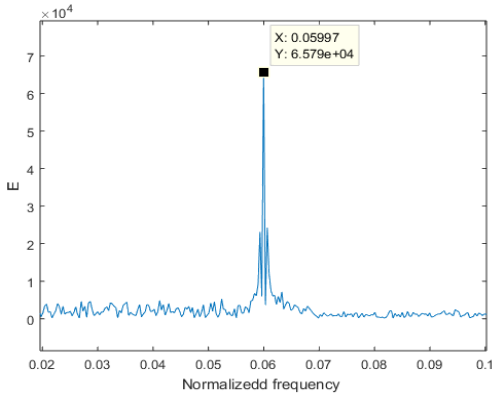

Graph 4.4: Silicon Steel Half Cylinder with Fins at 34Hz

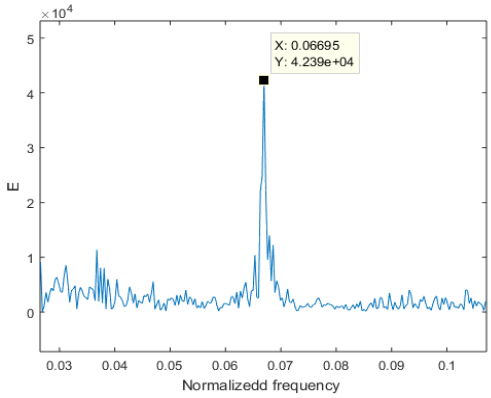

Graph 4.5: Silicon Steel Half Cylinder with Fins at 40Hz

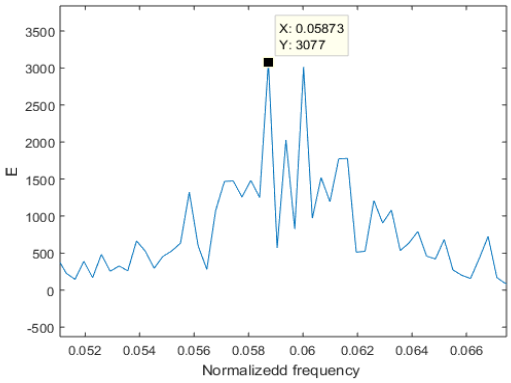

Graph 4.6: Silicon Steel Half Cylinder without Fins at 16Hz

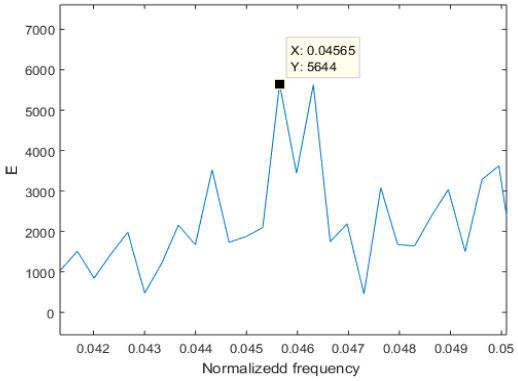

Graph 4.7: Silicon Steel Half Cylinder without Fins at 22Hz

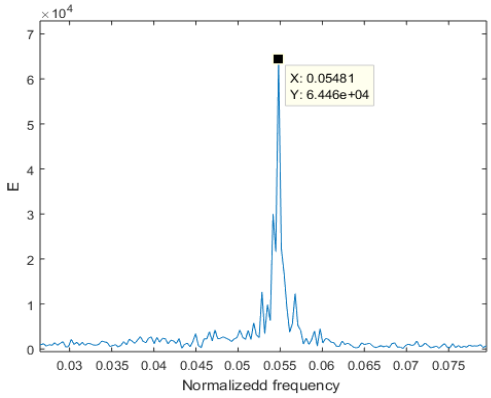

Graph 4.8: Silicon Steel Half Cylinder without Fins at 28Hz

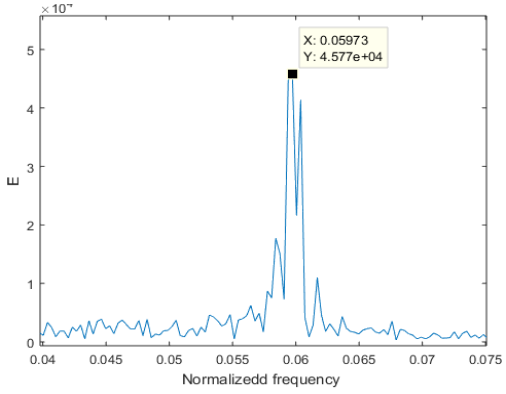

Graph 4.9: Silicon Steel Half Cylinder without Fins at 34Hz

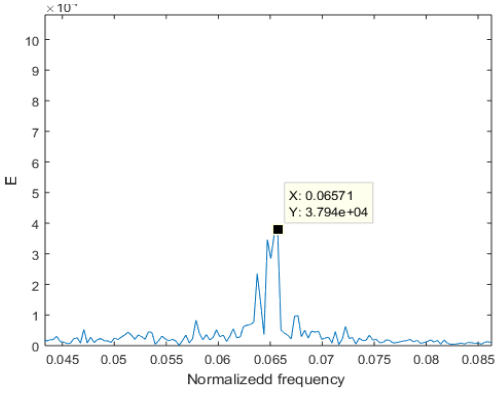

Graph 4.10: Silicon Steel Half Cylinder without Fins at 40Hz

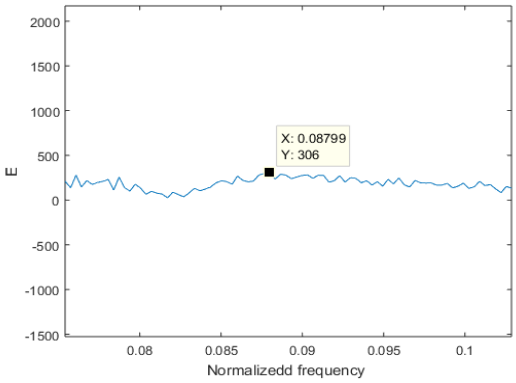

Graph 4.11: Stainless Steel Half Cylinder with Fins at 16Hz

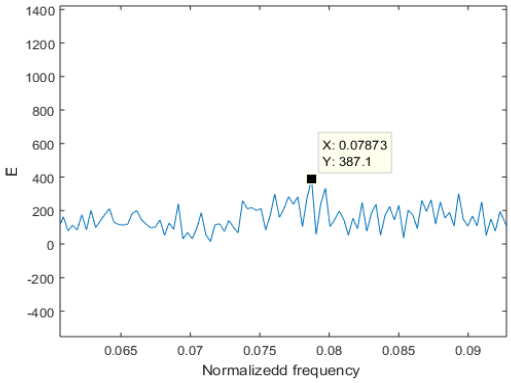

Graph 4.12: Stainless Steel Half Cylinder with Fins at 22Hz

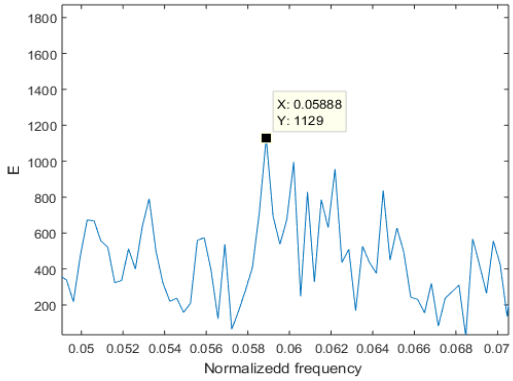

Graph 4.13: Stainless Steel Half Cylinder with Fins at 28Hz

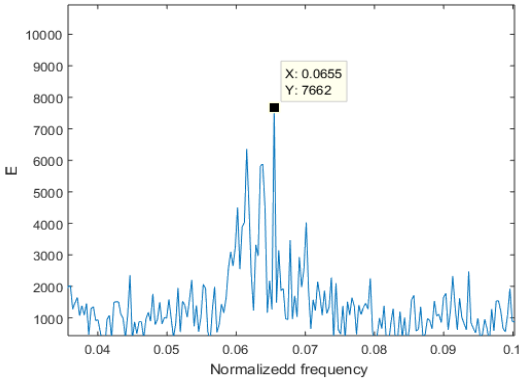

Graph 4.14: Stainless Steel Half Cylinder with Fins at 34Hz

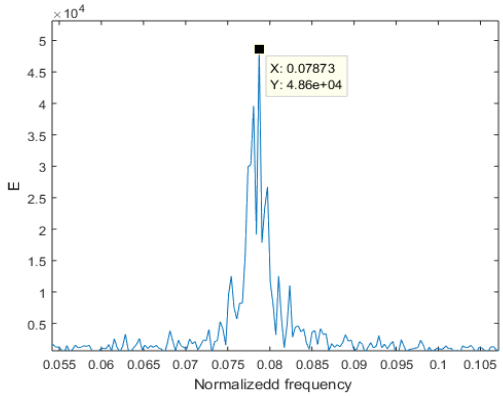

Graph 4.15: Stainless Steel Half Cylinder with Fins at 40Hz

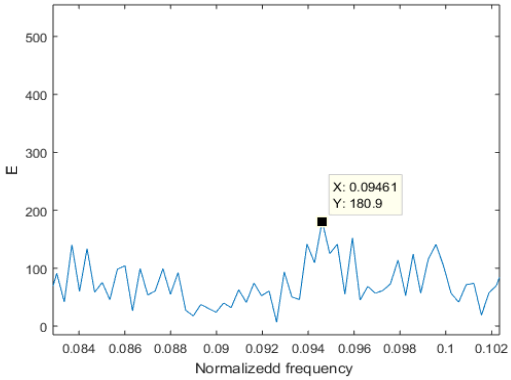

Graph 4.16: Stainless Steel Half Cylinder without Fins at 16Hz

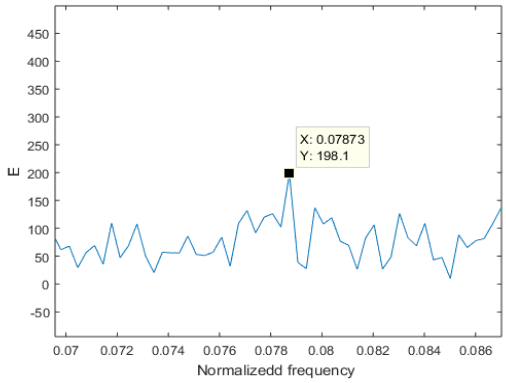

Graph 4.17: Stainless Steel Half Cylinder without Fins at 22Hz

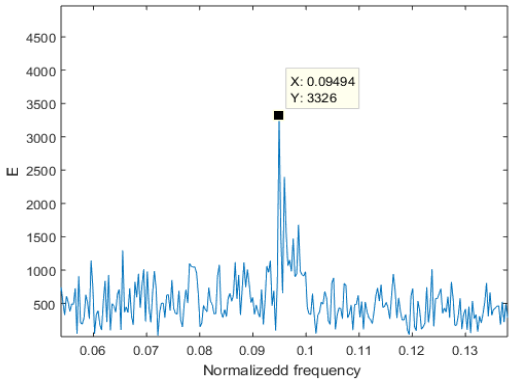

Graph 4.18: Stainless Steel Half Cylinder without Fins at 28Hz

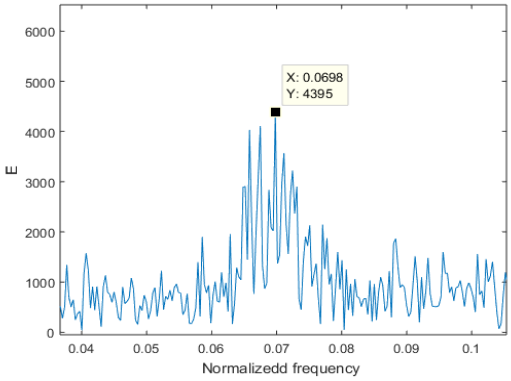

Graph 4.19: Stainless Steel Half Cylinder without Fins at 34Hz

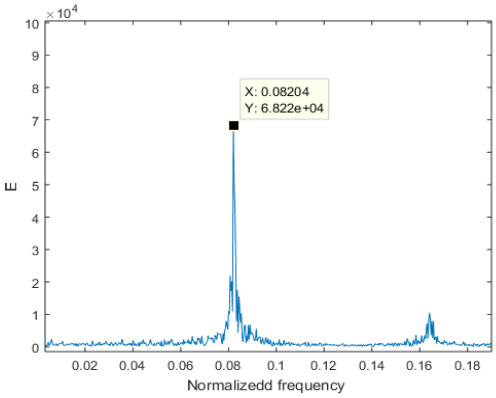

Graph 4.20: Stainless Steel Half Cylinder without Fins at 40Hz

- Figures ranging from graph 4.1 to graph 4.20 show how peak value of frequency changes with different frequencies of pump for two different bluff bodies mounted on two cantilever beams separately. For same Reynold number, the peak frequency values are greater for stainless steel cantilever beam as compare to silicon steel cantilever beam. All above graphs from graph 4.1 to graph 4.20 are shown below in table along with their corresponding pump frequencies and Reynold number.

Table 4.1: Frequency of flapping body at different Reynolds number

Pump Frequency (Hz)	Reynold Number	Peak Frequency of Silicon		Peak Frequency of Stainless Steel	
		Finned Cylinder	Unfinned Cylinder	Finned Cylinder	Unfinned Cylinder
16	1200	0.01438	0.05873	0.08799	0.09461
22	1600	0.04792	0.04565	0.07873	0.07873
28	1900	0.05218	0.05481	0.05888	0.09494
34	2300	0.05997	0.05973	0.0655	0.0698
40	2800	0.06695	0.06571	0.07873	0.08204

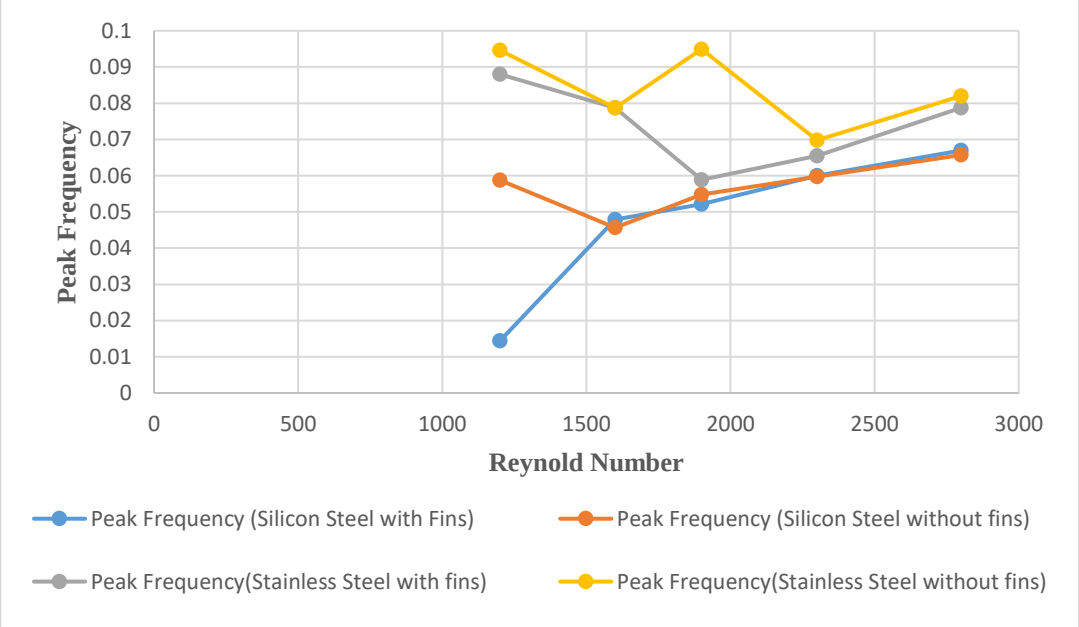

Graph 4.21: Flapping body frequency at different Reynold numbers

- From table 4.1 and graph 4.21, it can be seen that peak frequency continuously increases with increase in Reynold number for silicon substrate with finned half cylinder.

- For silicon substrate with unfinned half cylinder, the peak frequency shows fluctuation when pump frequency changes.
- Steel substrate with finned half cylinder also shows fluctuations. Peak frequency decreases at first and then it goes on increasing.
- Steel substrate with finned half cylinder has maximum peak frequency but there is no continuous increment but instability because of continuous fluctuations at each pump frequency.

4.2 AMPLITUDE VARIATIONS WITH REYNOLD NUMBER

4.2.1 Reynold number =1200

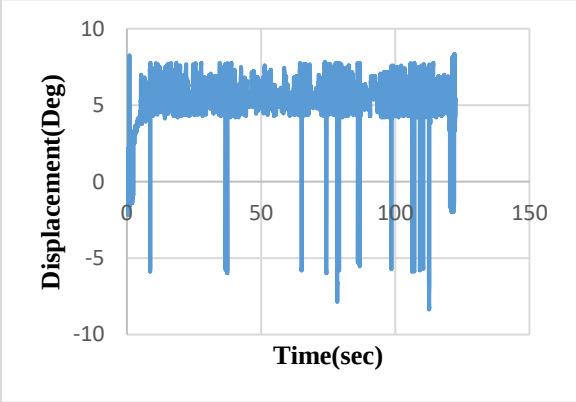

Graph 4.22: Silicon Steel Half Cylinder with Fins

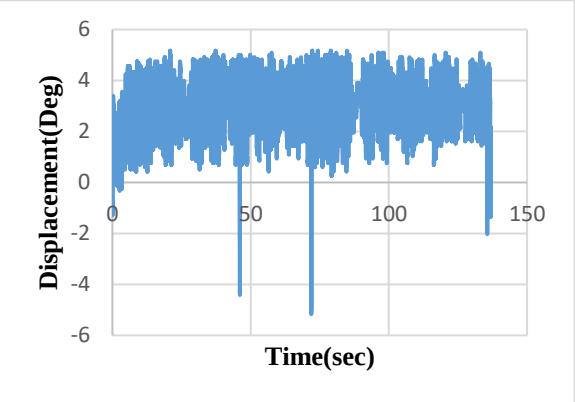

Graph 4.23: Silicon Steel Half Cylinder without Fins

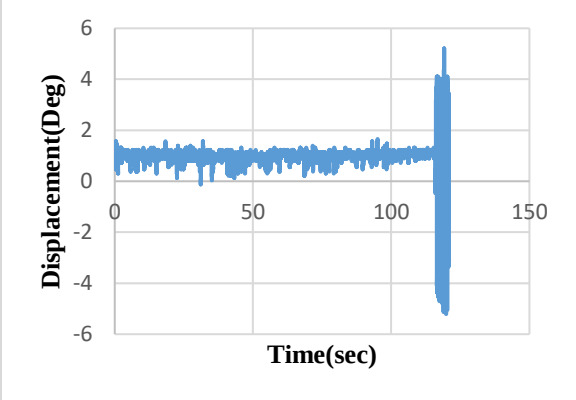

Graph 4.24: Stainless Steel Half Cylinder with Fins

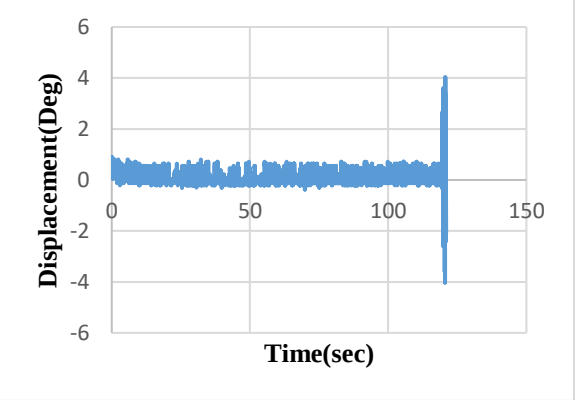

Graph 4. 25: Stainless Steel Half Cylinder without Fins

- When Reynold number is 1200, it can be seen from above graphs (Graph 4.22 to Graph 4.25) that amplitude is maximum when silicon steel cantilever beam is used with finned half cylinder mounting on it (Graph 4.22) thereby producing maximum oscillations or flapping. While stainless steel cantilever beam with unfinned half cylinder mounting on it gives minimum value of amplitude (Graph 4.25) thereby producing minimum flapping.

4.2.2 Reynold number =1600

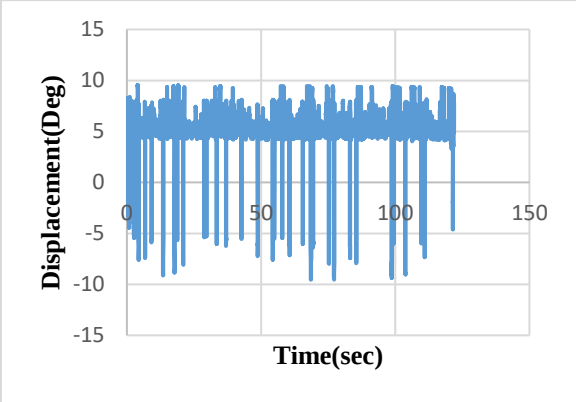

Graph 4.26: Silicon Steel Half Cylinder with Fins

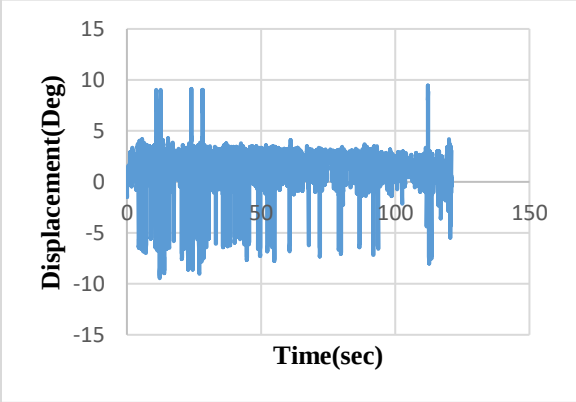

Graph 4.27: Silicon Steel Half Cylinder without Fins

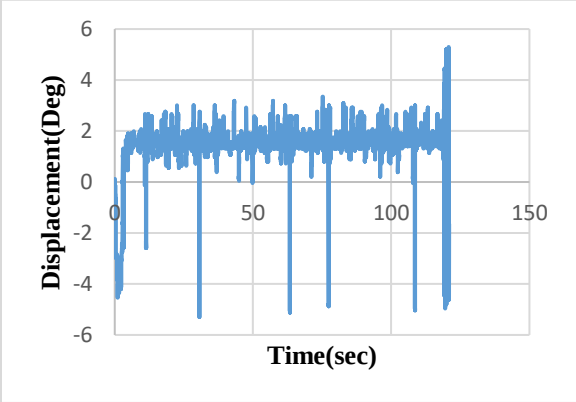

Graph 4.28: Stainless Steel Half Cylinder with Fins

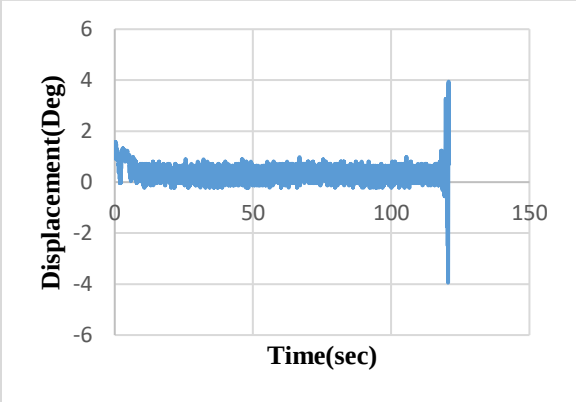

Graph 4.29: Stainless Steel Half Cylinder without Fins

- Figures ranging from graph 4.26 to graph 4.29 show that when Reynold number is 1600 then maximum amplitude is depicted in silicon steel cantilever beam when finned half cylinder is mounted on it (Graph 4.26). It gives maximum flapping thereby making it more suitable for IOT applications. At same Reynold number, remaining three cases gives minimum flapping due to minimum amplitude depicted

in them. Stainless steel with unfinned half cylinder (Graph 4.29) makes its amplitude to the minimum thereby making it inappropriate to give maximum oscillations for energy harvesting applications.

4.2.3 Reynold number =1900

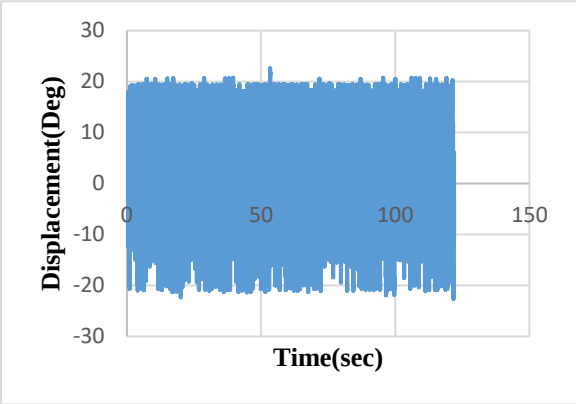

Graph 4.30: Silicon Steel Half Cylinder with Fins

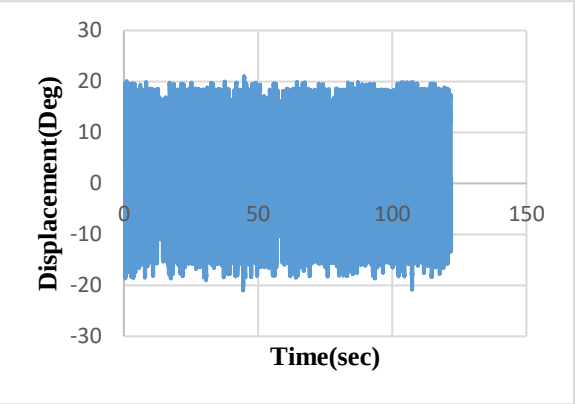

Graph 4.31: Silicon Steel Half Cylinder without Fins

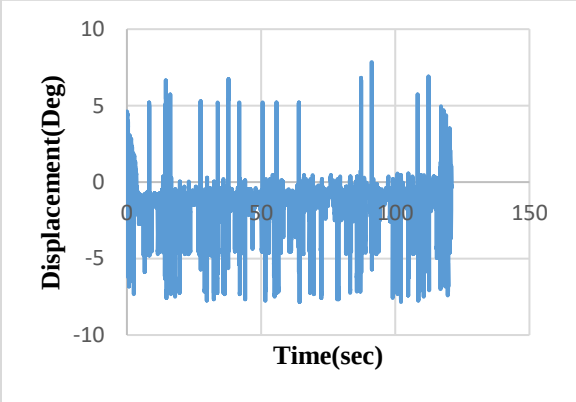

Graph 4.32: Stainless Steel Half Cylinder with Fins

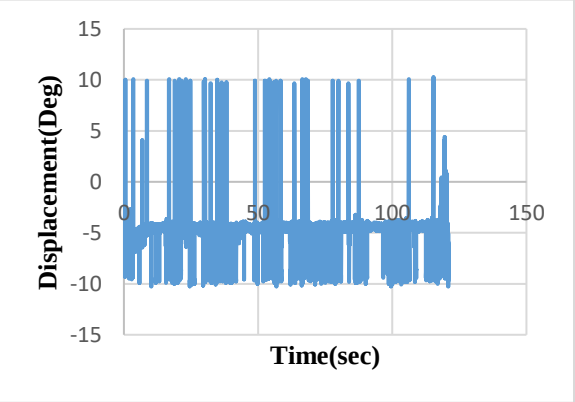

Graph 4.33: Stainless Steel Half Cylinder without Fins

- Above graphs show that when Reynold number is 1900 then maximum amplitude is obtained in silicon steel cantilever beam with finned half cylinder assembled on it (Graph 4.30). Maximum amplitude gives maximum oscillations making it desirable to harvest energy from motion giving high energy output. While stainless steel with finned half cylinder positioned on it gives minimum amplitude (Graph 4.32). Silicon with unfinned half cylinder and stainless steel with unfinned cylinder also gives low amplitude as compare to that of silicon steel with finned half cylinder mounting on it.

4.2.4 Reynold number =2300

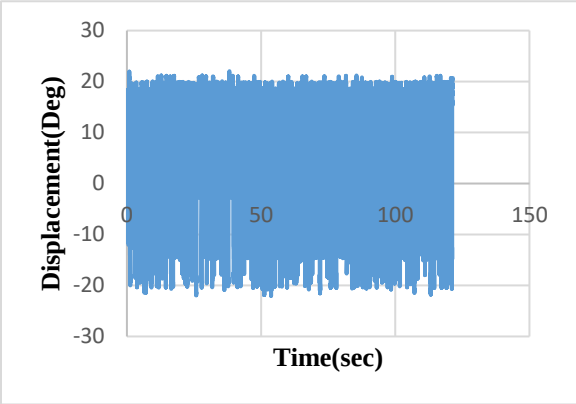

Graph 4.34: Silicon Steel Half Cylinder with Fins

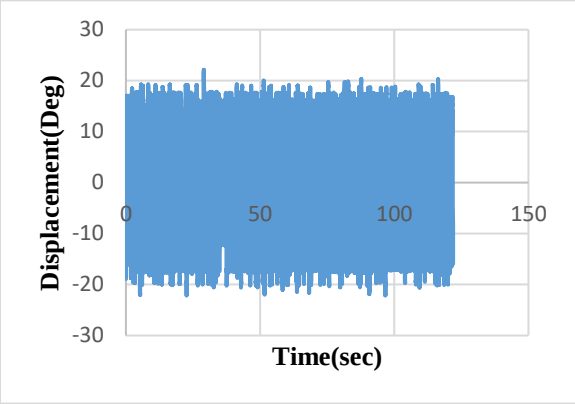

Graph 4.35: Silicon Steel Half Cylinder without Fins

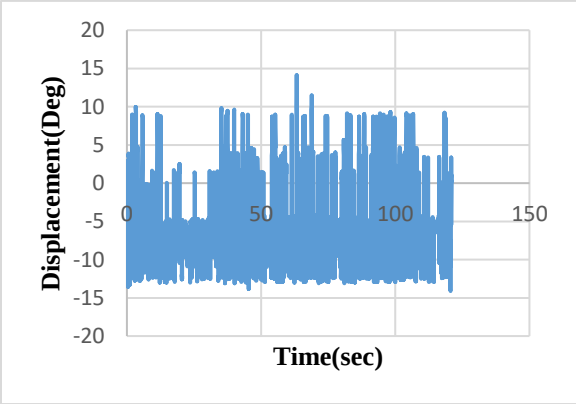

Graph 4.36: Stainless Steel Half Cylinder with Fins

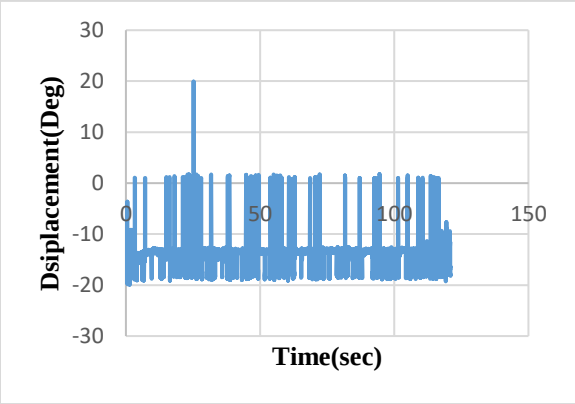

Graph 4.37: Stainless Steel Half Cylinder without Fins

- It is observed that maximum amplitude is depicted in silicon steel with finned half cylinder mounted on it (Graph 4.34). Maximum amplitude gives maximum energy output due to maximum flapping when used in energy harvesting applications. Stainless steel with unfinned half cylinder (Graph 4.37) gives minimum amplitude making it unsuitable for energy harvesting IOT applications. Silicon steel cantilever beam has maximum flapping than stainless steel cantilever beam.

4.2.5 Reynold number =2800

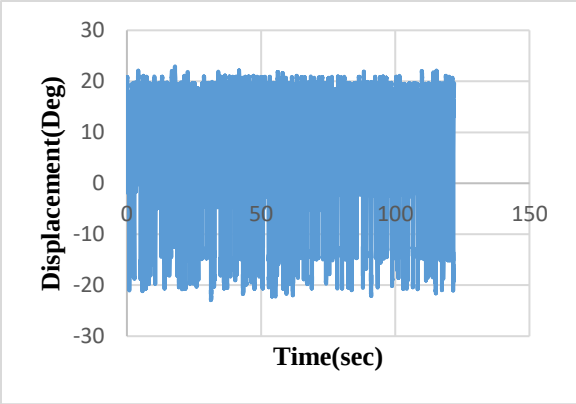

Graph 4.38: Silicon Steel Half Cylinder with Fins

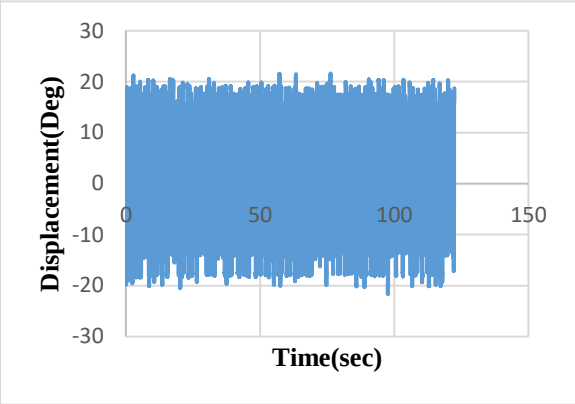

Graph 4.39: Silicon Steel Half Cylinder without Fins

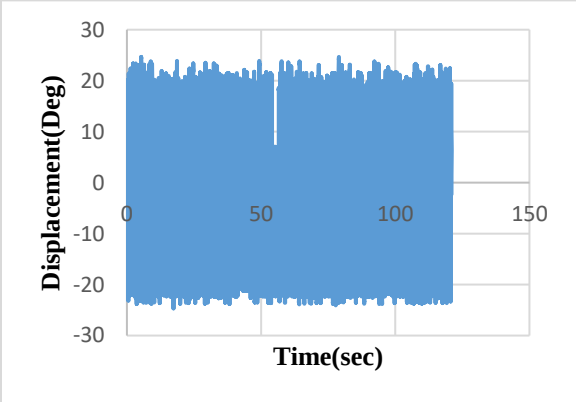

Graph 4.40: Stainless Steel Half Cylinder with Fins

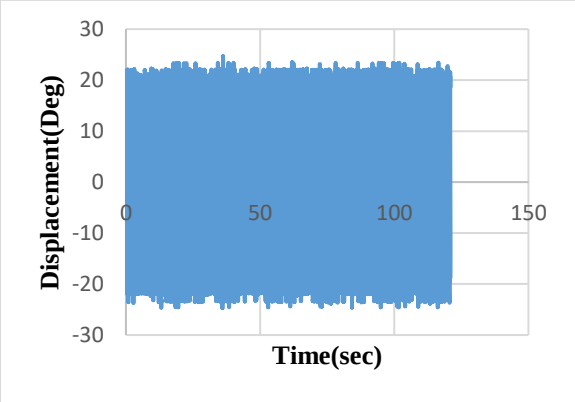

Graph 4.41: Stainless Steel Half Cylinder without Fins

- Above graphs represent that when Reynold number is 2800 then silicon steel with finned cylinder and stainless steel with both finned and unfinned cylinders give almost same variations in amplitude (Graph 4.38, 4.40 and 4.41). These three cases gives maximum flapping due to more vortices created at high Reynold number. While graph 4.39 shows that when silicon steel with unfinned half cylinder is used then amplitude is little less as compare to all other three cases. High Reynolds numbers indicate that inertial forces dominate over viscous forces, leading to turbulent flow. In a turbulent flow, disturbances such as those caused by a bluff body or a cantilever beam are more likely to be amplified, leading to more vigorous flapping and increased vortex shedding.

CONCLUSIONS

To harvest energy, an experiment is conducted in the water flow channel. Silicon steel and stainless steel are used as two different cantilever beams having length of 150mm each. Rectangular holes are cut in the stainless steel cantilever beam to make its weight equal to the weight of silicon steel cantilever beam. Two different bluff bodies are used i.e. half cylinder with fins and half cylinder without fins. Silicon steel cantilever is used because it gives rise to the more drag. More drag created by the bluff bodies that disturbs the flow of the water and more vortices are created which can result in electric current generation when electric eels are used.

From above results we concluded that peak frequency increases with increase in Reynold number corresponding to pump frequencies. Maximum peak frequency is depicted in the stainless steel when half cylinder without fins is mounted on it as compare to half cylinder with fins mounted on same cantilever beam. Peak frequency in stainless steel cantilever beam is fluctuating which lead to instability in performance. We also concluded that overall peak frequency for silicon steel cantilever beam is less as compare to stainless steel cantilever beam but in silicon steel there is continuous increment in peak frequency without fluctuations. When half cylinder with fins is mounted on silicon steel cantilever beam then peak frequency value is greater as compare to unfinned half cylinder mounted on same cantilever beam. Although at some points the unfinned half cylinder mounted on silicon steel has higher values but overall increment in frequency is very less (from 0.05873 to 0.06571) as compare to increment in frequency (from 0.01438 to 0.06695) when finned cylinder is used. Peak frequency is continuously increasing when silicon steel cantilever beam is used while stainless steel has irregular variations in peak frequency as seen from figure 4.21.

For amplitude, it is concluded that amplitude increases over the time when pump frequency and corresponding Reynold number are increasing. When half cylinder with fins is mounted on the silicon steel cantilever beam, we observed that amplitude fluctuations are greater as compare to unfinned half cylinder mounted on same cantilever beam. Therefore,

use of fins increases the flapping of bluff body thereby increasing the amplitude of vibrations. For stainless steel cantilever beam, the amplitude fluctuations are greater when finned half cylinder is mounted on it as compare to unfinned half cylinder mounting on same cantilever beam.

Conclusively, we can see that silicon cantilever beam with finned half cylinder mounted on it has maximum amplitude as compare to all other cases. It gives maximum amplitude at pump frequency of 40Hz i.e. 20-25degree. Although silicon steel has less peak frequency than stainless steel but continuous increment in peak frequency with increase in pump frequency make it viable solution for harvesting energy. Fluctuations make stainless steel less predictable for performance thereby giving priority to silicon steel having less fluctuations and consistent increase in peak frequency.

5.1 FUTURE RECOMMENDATIONS

- For future, it is recommended to use wind tunnel instead of water channel for same testing procedure. In water channel, water has high density and high damping effect which has detrimental effect on maximum frequency and amplitude of oscillations.
- It is also recommended to determine natural frequency of materials used in assembling the setup. This enables to identify the reasons for variations in behavior of vibrations.
- Bluff body should be finned. Fins have the potential to increase vorticity and turbulence, which could result in vortex shedding and oscillations with a greater frequency and possibly larger amplitude. The fins enhance the interaction between the fluid and the cantilever beam by effectively disrupting the flow.

REFERENCES

[1] A. Aabid, "A Systematic Review of Piezoelectric Materials and Energy Harvesters for Industrial Applications," *MDPI*, pp. 22-27, 2021.

[2] T. Shi, "Performance of an omnidirectional piezoelectric wind energy harvester," *WILEY*, pp. 1177-1179, 2021.

[3] A. Naqvi, "Energy Harvesting from Fluid Flow Using Piezoelectric Materials: A Review," *MDPI*, pp. 27-35, 2022.

[4] M. Zhang, "Influence of predefined angle of attack on piezoelectric energy harvesting from transverse galloping of different bluff bodies," *Applied Ocean Research*, pp. 12-16, 2022.

[5] M. Hamlehdar, "Energy harvesting from fluid flow using piezoelectrics: A critical review," *Renewable Energy*, pp. 1835-1838, 2019.

[6] M. C. A, " An Experimental Study of Vortex Shedding Behind a Bluff Body in a Water Channel," *International Journal of Engineering Research & Technology (IJERT)*, vol. 05, no. 06, pp. 707-707, 2016.

[7] W. KenChin, "Enhancement of Energy Harvesting Performance by a Coupled Bluff Splitter Body and PVEH Plate through Vortex Induced Vibration near Resonance," *MDPI*, pp. 28-31, 2017.

[8] K. Lei, "A semicircular wall for harvesting wind energy from vortex-induced vibration and galloping," *Ocean Engineering*, pp. 10-11, 2023.

[9] J. Wang, " High-performance piezoelectric wind energy harvester with Y-shaped attachments," *Energy Conversion and Management,* pp. 650-652, 2019.

[10] J. Wang, "Enhanced performance of piezoelectric energy harvester by two asymmetrical splitter plates," *Ocean Engineering*, pp. 10-12, 2023.

[11] G. Hu, "Experimental investigation on the efficiency of circular cylinder-based wind energy harvester with different rod-shaped attachments," *Applied Energy*, pp. 687-689, 2018.

[12] J. Wang, "A cross-coupled dual-beam for multi-directional energy harvesting from vortex induced vibrations," *Smart Materials and Structures*, pp. 5-8, 2019.

[13] A. Abdelkef, "An energy harvester using piezoelectric cantilever beams undergoing coupled bending–torsion vibrations," *Smart Materials and Structures*, pp. 10-11, 2011.

[14] X. Shan, "Enhancing Performance of a Piezoelectric Energy Harvester System for Concurrent Flutter and Vortex-Induced Vibration," *MDPI*, pp. 16-19, 2020.

[15] R. Song, " A study of vortex-induced energy harvesting from water using PZT piezoelectric cantilever with cylindrical extension," *Ceramics International* , pp. 5-6, 2015.